Role of resonances and quantum-mechanical interference in the generation of above-threshold-ionization spectra

V. C. Reed and K. Burnett
Clarendon Laboratory, Department of Physics, University of Oxford, Parks Road, Oxford OX1 3PU, United Kingdom
(Received 26 November 1990)

A general technique for modeling the behavior of an atom in the presence of a laser field is described. This involves the integration of the time-dependent Schrödinger equation in the Kramers-Henneberger frame. Results are presented for a one-dimensional calculation for a model hydrogen atom across a range of frequencies and intensities. The resultant peaks in the photoelectron spectra produced are shown to be partly the result of Stark-shifted bound-state multiphoton resonances. The spectra also contain rainbow features due to interference between the electron amplitude generated on the rising and falling edge of the pulse. These rainbow features are a purely time-dependent effect that can only be easily reproduced in time-dependent calculations.

I. INTRODUCTION

With the advent of higher-intensity subpicosecond lasers, the picture of an above-threshold-ionization (ATI) spectrum, consisting of simple, well-defined peaks, each separated by the photon energy, has had to be modified. Instead, it has been found that satellite lines to the main peaks occur and the positions of the main peaks themselves vary with intensity.[1-3] Since the intensities involved in the experiments exceed those that would allow treatment using finite-order perturbation theory, much of the theoretical study of these features has had to rely on numerical calculation.

Much theoretical work has been undertaken in an attempt to explain the features of ATI spectra,[4] but the time-dependent structure of the laser pulse has in the main been ignored. In depth analyses of the ATI structure have been performed that rely on Floquet theory and deal precisely with the internal structure of the atom and these have then been compared with experimental data.[5] These results are based on time-independent methods and the spectra are composed of independent components resulting from different intensities. Such methods cannot, however, reproduce some characteristics of the observed spectra that arise specifically because of the time-varying electric field. In particular, the interference between amplitudes produced at different times in the pulse cannot be easily included. The aim of our work is to overcome the restriction of this time-independent work and present the results of time-dependent numerical calculations. Using these results, various characteristics of the spectra will be explained, including those that do not occur in the time-independent picture. Experimentally, the observed spectra will depend on both the temporal and spatial structure of the laser pulse. In this paper, the role of the time-varying nature of the electric field is examined. The part that averaging over the spatial extent of the laser beam plays is quite distinct from the role that the time dependence of the pulse plays. We are not, at present, concerned with this spatial averaging, but are limiting ourselves solely to looking at the characteristics of the ATI spectra that arise due to the time-varying electric field.

There have been several time-dependent numerical calculations performed to date, which have yielded various results across a wide range of experimental parameters.[6-8] The techniques employed rely on some method of solving a time-dependent Schrödinger equation. The nature of the problem, however, imposes a restriction on the calculations that can be performed in the time domain: as the atom ionizes, it produces fast-moving electron wave packets that must be tracked in time and the calculation therefore necessitates the use of a large amount of superconducting time. Our method, which makes use of the Kramers-Henneberger (KH) frame to minimize this difficulty, is compared in Sec. II with those used by other workers. It has been found that the KH frame offers significant advantages compared to the laboratory frame. To our knowledge, ours is the first calculation to take place in the KH frame. We have previously used it to study long-pulse ATI spectra,[6] over-the-barrier ionization,[6] and the suppression of ionization in ultraintense laser fields.[9] The KH frame has been also used to facilitate the physical interpretation of high-field ionization suppression[10,11] and to study time-independent scattering phenomena.[12]

In Sec. III, results of the calculation are outlined for regions of parameter space where there are no resonances in the coupling from the ground state to the excited states of the atom; instead the atom ionizes by passing through virtual levels. In this case, provided the total ionization of the atom is small, subpeaks are observed in the electron energy spectrum. These subpeaks are interpreted in terms of interference between the ionization amplitude produced on the rising and falling edges of the smooth laser pulse that is used.

Section IV deals with ionization when excited levels of the atom are resonant, or nearly resonant, with the dressed ground state. Various multiphoton resonances that occur are identified and the effect of these on the structure of the ATI spectrum is examined. For decreasing laser frequency, the number of resonances that can

occur in the laser pulse increases and for a pulse of low frequency compared to the atomic frequency, a typical ATI peak is examined. In an experiment, both the interference and resonance structure of the ATI spectrum will be affected by the spatial extent of the laser beam. It is not, however, the aim of this paper to examine the role of the *spatial* structure of the pulse, but only the effect of the *time variation* of the pulse.

Finally Sec. V deals with the conclusions that have been drawn from the calculations and outlines various avenues of investigation that could be pursued further.

II. THE NUMERICAL CALCULATION

Finite-order perturbation theory and other approximate analytical studies are inadequate to address many of the issues relevant to ATI. This has led to an increasing amount of interest in direct numerical integration of the Schrödinger equation, and such time-dependent work has been pursued both in one and three dimensions.[6–9] In numerical calculations that rely solely on the direct integration of the Schrödinger equation, correctly modeling the ionized electron wave packet presents problems: the evolving wave packet is still in the presence of the external laser field and it must not be allowed to "hit" the edge of the grid of integration. This imposes a severe restriction on the calculation. If a wave packet reaches the boundary, it will be reflected back and undergo further interaction with the core of the potential in the presence of the field. To avoid this, the grid must be made large enough so that the fastest moving wave packet never reaches the edge. Even for relatively short pulses this means an extremely large grid must be used. The standard calculation involves matrix inversion at every time step, resulting in an approximate N^3 dependence for the amount of CPU time needed, where N is the number of grid points. Hence increasing the pulse length in the calculation will drastically increase the computer time needed.

To reduce the severity of this problem, one can use the Kramers-Henneberger frame.[13,14] This is the frame of motion of a free-electron wave packet in the applied electric field. The KH frame has been used previously in time-dependent Floquet calculations,[12] but, to our knowledge, we have performed the first time-dependent calculations to actually take place in the KH frame. We have already carried out calculations in the KH frame to examine the transition to over-the-barrier ionization[6] and also to study ionization suppression in ultraintense laser pulses.[9] In addition, the KH frame has been used to interpret how ionization suppression occurs.[10,11] The wave function in the laboratory (lab) and Kramers-Henneberger (KH) frames are related by the unitary transformation

$$\phi_{\mathrm{KH}}(\mathbf{r},t)=U_1U_2\psi_{\mathrm{lab}}(\mathbf{r},t)\ , \tag{2.1}$$

where $\psi_{\mathrm{lab}}(\mathbf{r},t)$ is in the $\mathbf{p}\cdot\mathbf{A}$ gauge. U_1 and U_2 are given by

$$U_1=\exp\left[\frac{iq^2}{2m\hbar}\int_{-\infty}^{t}d\tau\ \mathbf{A}^2(\tau)\right] \tag{2.2}$$

and

$$U_2=\exp\left[\frac{-q}{m}\int_{-\infty}^{t}d\tau\ \mathbf{A}(\tau)\cdot\nabla\right]\ , \tag{2.3}$$

where $\mathbf{A}$ is the vector potential of the laser field.

The Schrödinger equation in the $\mathbf{p}\cdot\mathbf{A}$ frame with an applied electric field is given by

$$i\hbar\frac{\partial\psi_{\mathrm{lab}}}{\partial t}(\mathbf{r},t)=-\frac{\hbar^2}{2m}\nabla^2\psi_{\mathrm{lab}}(\mathbf{r},t)+\frac{i\hbar q}{m}\mathbf{A}\cdot\nabla\psi_{\mathrm{lab}}(\mathbf{r},t)+\frac{q^2A^2}{2m}\psi_{\mathrm{lab}}(\mathbf{r},t)+V(\mathbf{r})\psi_{\mathrm{lab}}(\mathbf{r},t)\ . \tag{2.4}$$

Application of the KH transformation to this equation produces the following version of the Schrödinger equation:

$$i\hbar\frac{\partial\phi_{\mathrm{KH}}}{\partial t}(\mathbf{r},t)=-\frac{\hbar^2}{2m}\nabla^2\phi_{\mathrm{KH}}(\mathbf{r},t)+V(\mathbf{r}+\boldsymbol{\alpha}(t))\phi_{\mathrm{KH}}(\mathbf{r},t)\ . \tag{2.5}$$

Hence U_1 is a phase-transformation operator which removes the A^2 term from the Schrödinger equation and U_2 represents a shift to the accelerated frame of reference. U_2 can be written in the form

$$U_2=\exp[\boldsymbol{\alpha}(t)\cdot\nabla]\ , \tag{2.6}$$

where $\boldsymbol{\alpha}(t)$ is given by

$$\boldsymbol{\alpha}(t)=-\frac{q}{m}\int_{-\infty}^{t}\mathbf{A}(\tau)d\tau\ . \tag{2.7}$$

Examining the transformed Schrödinger equation, one sees that the effect of the laser pulse now appears as a time dependence of the potential. The potential now oscillates at the frequency of the applied laser pulse and with an amplitude given by $\boldsymbol{\alpha}(t)$, which is the classical displacement of a free electron in the laser field.

This localization of the effect of the laser field is the most important feature of the KH frame in these calculations. Once an electron wave packet is outside the range of the potential, then it is no longer in the electric field and can be described as a simple plane wave. Such a free-electron wave packet can therefore be allowed to travel to the edge of the grid, reflect from the boundary, and travel back up to the edge of the range of the potential. This reduces the size of the required grid by almost a factor of 2, which, for an N^3 time dependence represents a reduction of nearly a factor of 8 for the length of the calculation. Hence calculations can be performed for correspondingly longer pulses than is possible in the laboratory frame.

The calculation that we have performed involved the direct time integration of the time-dependent Schrödinger equation in the KH frame. The electric field is treated classically within the dipole approximation as a coherent pulse with no phase or amplitude fluctuations. At present the calculation is in one dimension, but the technique is, of course, not limited to one dimension only. However, such calculations are particularly rapid.

At the beginning of the pulse, both the $\mathbf{A}$ and $\mathbf{E}$ fields are zero and the initial bound state of the system is found

by solving the field-free time-independent Schrödinger equation (in atomic units), i.e.,

$$W\xi(x)=-\frac{1}{2}\frac{d^2\xi}{dx^2}(x)+V(x)\xi(x)\ , \tag{2.8}$$

which, because of the zero field, is the same in both the laboratory and the KH frame. The wave function $\xi(x)$ is found by a Numerov method,[15] and initially W_g the ground-state energy of the potential is found.

The potential used is given by[7]

$$V(x)=\frac{-1}{(1+x^2)^{1/2}}\ . \tag{2.9}$$

This was chosen because it has a Coulombic tail and produces a Rydberg series of bound eigenstates. For the size of the grid used for most of the following calculations, the ground state has a binding energy of -0.6698 a.u. (18.41 eV) and has 71 bound states. In addition, parity is a good quantum number for this potential.

The laser pulse is modeled by the electric field given by

$$E(t)=E_0\sin(\omega t)\sin^2\left[\frac{\pi t}{T}\right]\ , \tag{2.10}$$

where T is the length of the pulse and ω is the angular frequency of the applied laser field. This corresponds to a pulse length of $2\pi N/\omega$, where there are N cycles of the laser field in the laser pulse. Using a smooth pulse such as this reduces the "switch-on" effects that populate the higher bound states of the atom.

The time-dependent Schrödinger equation that is solved at each time step is the one-dimensional version of Eq. (2.5) in atomic units,

$$i\frac{\partial\phi_{\rm KH}}{\partial t}(x,t)=-\frac{1}{2}\frac{\partial^2\phi_{\rm KH}}{\partial x^2}(x,t)+V(x+\alpha(t))\phi_{\rm KH}(x,t)\ , \tag{2.11}$$

where the displacement of the potential, $\alpha(t)$, is calculated analytically from Eq. (2.7).

The time evolution is performed using a Crank-Nicholson finite-difference iterative method[15] on a Convex C120 vector processor, operating at approximately one-eighth the speed of a Cray 1S computer. The particular routine used is accurate to second order in both Δx and Δt, which are the grid spacing and time step, respectively. At the end of the pulse, the evolved wave function is transformed back to the $\mathbf{p}\cdot\mathbf{A}$ frame using the inverse KH transformation. As the vector potential is zero at the end of the pulse envelope for a pulse symmetrical in $\mathbf{E}$, then the $\mathbf{p}\cdot\mathbf{A}$ and $\mathbf{d}\cdot\mathbf{E}$ frames are coincident, so no transformation to the $\mathbf{d}\cdot\mathbf{E}$ frame need be applied.

To find the energy spectrum of the ionized photoelectrons, the evolved wave function is overlapped with the continuum-energy eigenstates. The continuum is modeled by an infinite, but discrete, set of eigenstates, which are solutions of Eq. (2.8) with positive eigenenergies. The continuum is discretized by the boundary conditions imposed by the edge of the grid, but for large enough grid sizes, this imposes no restrictions on the calculation. The energy spectrum is defined, following Javanainen, Eberly, and Qichang Su,[7] according to the formula

$$P\left[\frac{W_{n-1}+W_n+W_{n+1}+W_{n+2}}{4}\right]=\frac{|\langle\xi_n(x)|\psi(x,T)\rangle|^2}{W_{n+1}-W_{n-1}}+\frac{|\langle\xi_{n+1}(x)|\psi(x,T)\rangle|^2}{W_{n+2}-W_n}\ . \tag{2.12}$$

This formula takes account of the large differences in population between adjacent states of opposite parity in the continuum.

The spacing between grid points is chosen to ensure that the eigenenergy-finding routine can adequately produce eigenfunctions up to the highest energy in the continuum that is required for the energy spectrum. The total size of the grid, and hence the total number of grid points used, is chosen so that the pulse is finished before the fastest moving electron wave packet reflects from the grid boundary and travels back into the region of interaction with the time-dependent potential. The time step is chosen so that there are enough time steps in one cycle of the oscillation of the highest energy free-electron wave packet to adequately follow its motion.

III. INTERFERENCE STRUCTURE IN THE ATI PEAKS

For sufficiently high frequencies, there are ranges of frequencies where the Stark shifts of the bound levels do not sweep any of the higher bound levels of the atom into multiphoton resonance with the ground state. In these regions, the positions of the main peaks in the energy spectra produced are given, to good accuracy, by the formula

$$W_n=W_g(0)+n\omega+W_p(T/2)\ . \tag{3.1}$$

Here $W_p(T/2)$ is the maximum Stark shift of the ground state, with respect to the continuum states. This is given approximately by the expression $-(E_0/2\omega)^2$ and $W_g(0)$ is the zero-field ionization energy of the atom.

In our calculation, the position of these peaks in the energy spectrum is independent of the length of the pulse; a longer length pulse merely has the effect of decreasing the width of the line. However, in addition to these main peaks, there occurs immediately to the right of the main peaks in the spectrum, a series of peaks of decreasing height with increasing energy that have positions which are dependent of the length of the pulse. The pattern of these subpeaks is similar for each of the main peaks in the spectrum.

These subpeaks only occur when a time-varying electric field is used. For square pulse calculations, there are subpeaks observable,[7] but they are due to ionization from higher bound states populated during the sharp "switch-on" of the pulse. The subpeaks observed with the smooth pulse are due to interference between the photoelectron amplitudes produced at the same laser intensity on the

rising and falling edge of the pulse. The use of any smooth pulse that results in a time-varying ground-state energy will produce such interference. To verify the nature of these peaks, a simple theory can be formulated that gives an estimate of the separation of these subpeaks.

For a nonresonant ionization process, the system, in the dressed-state picture, can be thought of as consisting of solely a ground state and a continuum. The intermediate states simply give rise to the slowly varying coupling between the initial and final states. For an n-photon ionization process from a pulse with an electric-field envelope defined in Eq. (2.10) above, the dressed ground-state energy will be

$$W_g(t)=W_g(0)+W_p(t)+n\omega \ . \tag{3.2}$$

Here, $W_g(0)$ is the zero-field ground-state energy, n is the number of photons absorbed during the ionization process, and $W_p(t)$ is the time-dependent Stark shift of the ground state with respect to the continuum. At the intensities that we are concerned with, the Stark shift can be approximated by the expression for the ponderomotive energy of the electron: for the case when the electric-field envelope is approximately constant over one oscillation of the laser field, then this can be written using Eq. (2.10) as

$$W_p(t)=-\frac{E_0^2}{4\omega^2}\sin^4\left[\frac{\pi t}{T}\right] . \tag{3.3}$$

Hence the energy of the electron liberated will vary as a function of time, depending on the laser intensity at which it ionizes. The ionized electron amplitude of a particular energy is produced both on the rising and falling edges of the pulse at the same value of the electric field—providing that ionization is not completed in the first half of the pulse. The two amplitudes can then interfere and produce a pattern, the constructive peaks of which are the subpeaks in the energy spectrum.[16]

The nonresonant n-photon interaction that results in the emission of the electron from the ground state to a state of energy W in the continuum can be approximated by a constant V_{gc}. Again, it is assumed that the amount of ionization in the pulse is low. (Decay can be included and does not affect the qualitative conclusion until it is very large, when it reduces the "fringe" contrast.) The two equations that determine the ground and continuum state amplitudes can then be taken to be

$$i\dot{a}_g(t)=W_g(t)a_g(t) \ , \tag{3.4}$$

$$i\dot{a}_W(t)=W(t)a_W(t)+V_{gc}a_g(t) \ . \tag{3.5}$$

Because of the slowly varying nature of the ground-state shift, the solution of Eq. (3.4) can be approximated by

$$a_g(t)=\exp\left[-i\int_0^t W_g(t')dt'\right] . \tag{3.6}$$

Substituting this into Eq. (3.5) and solving it produces an expression for the probability amplitude at the end of the pulse at an energy W in the continuum given by

$$a_W(T)=-iV_{gc}\exp(-iWT)\int_0^T\exp[i\phi(t)]dt \ , \tag{3.7}$$

where

$$\phi(t)=Wt-i\int_0^t W_g(t')dt' \ . \tag{3.8}$$

The integral in Eq. (3.7) can be approximated using the method of stationary phase. This method relies on the fact that for each value of the variable W, the energy in the continuum, there are two points during the laser pulse, t_s and $T-t_s$, which dominate the ionized wave amplitude at a given energy. These stationary phase points are in effect the local resonance points determined by

$$W=W_g(0)+n\omega+W_p(t_s) \ . \tag{3.9}$$

The ionization from these two points interferes and an interference pattern is produced that is a function of the energy of the continuum state; these are the subpeaks in the ATI spectrum. Thus Eq. (3.7) can be written in the form

$$a_W(T)\propto 1+\exp\{i[\phi(T-t_s)-\phi(t_s)+\pi/2]\} \ . \tag{3.10}$$

Because of the dependence on intensity of the ionization rate, the spectrum is dominated by the ionization that occurs at, or close to, the peak of the pulse. This fact allows Eq. (3.3) to be rewritten, close to the peak of the pulse, as

$$W_p(t)=\frac{-E_0^2}{4\omega^2}\sin^4\left[\frac{\pi t}{T}\right]\approx\frac{-E_0^2}{4\omega^2}+\beta\left[t_s-\frac{T}{2}\right]^2 , \tag{3.11}$$

where $\beta=E_0^2/(8N^2)$. Equation (3.10) can then be rewritten as

$$a_W(t)\propto 1+\exp\left\{i\left[\frac{-4}{3}\beta\left[t_s-\frac{T}{2}\right]^3+\frac{\pi}{2}\right]\right\} . \tag{3.12}$$

This gives a total probability of ionization into the continuum state of energy W of the form

$$|a_W(T)|^2\propto 1+\cos\left[\frac{4\beta}{3}\left[\frac{\Delta W}{\beta}\right]^{3/2}-\frac{\pi}{2}\right] . \tag{3.13}$$

Here, ΔW is the difference in energy between W, the continuum-state energy, and the energy of the electrons ionized at the peak electric field. Thus the maxima in the spectrum are predicted to be at the energies

$$W=W_g(0)+n\omega-\frac{E^{0^2}}{4\omega^2}+\left[\frac{3\pi}{8\beta}\right]^{2/3}\beta(4m+1)^{2/3} , \tag{3.14}$$

where $m=0,1,2,3,\ldots$ and the minima at the energies

$$W=W_g(0)+n\omega-\frac{E_0^2}{4\omega^2}+\left[\frac{3\pi}{8\beta}\right]^{2/3}\beta(4q-1)^{2/3} , \tag{3.15}$$

where $q=1,2,3,\ldots$.

Hence the dependence of the subpeaks on the length of the pulse and the electric field arises through β. However, β is independent of the angular frequency and thus the peak separation is also independent of this.

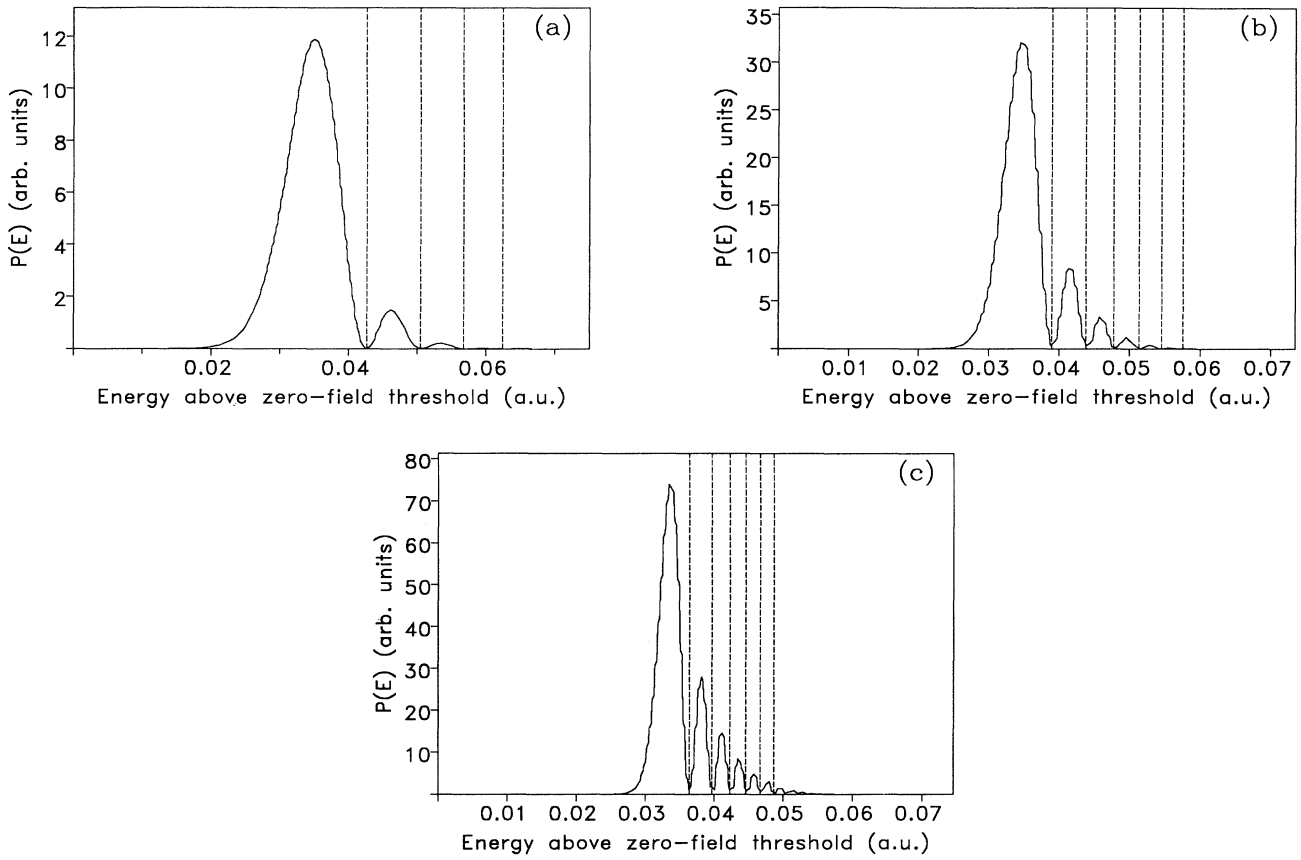

FIG. 1. Energy spectra from pulses with angular frequency $\omega=0.182$ (0.25 μm) and peak electric field, $E_0=0.053$ ($\approx 10^{14}$W/cm^2), with pulse lengths (a) 64 cycle (53 fs), (b) 128 cycle (106 fs), (c) 240 cycle (200 fs). The vertical dashed lines represent the predicted positions of the interference minima from Eq. (3.15) with the maximum ground-state Stark shift adjusted.

The magnitude of the subpeaks will depend on the positions of the stationary-phase points with respect to the peak of the pulse. The ionization amplitude is a maximum at the peak of the field where $t_s=T/2$ and the two points of stationary phase coincide. At this point the stationary-phase method will be invalid. Away from this maximum, the magnitude of the peaks in the photoelectron energy spectrum decreases with increasing energy, because the peak magnitude is inversely proportional to the rate of change of slope of the pulse envelope, hence giving large magnitudes towards the peak of the pulse.

A range of parameters has been used to test the validity of this theory with angular frequencies between 456 and 145 nm, and intensities in the region of 10^{14} W/cm^2. Intensities in this region have been chosen because the electric field is large enough to produce a noticeable quantum-interference pattern, but small enough that ionization over the resultant potential barrier of the atomic and laser fields is negligible.[6,17] For our potential, over-the-barrier ionization is possible from the ground state at an intensity of approximately 5×10^{14} W/cm^2.

Figures 1(a)–1(c) are a series of plots of the first ATI peaks for pulses of identical angular frequencies and intensities, but varying pulse lengths. It can be seen that the vertical lines on the plots, which represent the predicted minima of the interference patterns, correspond, to good precision, to the observed ones for all the different pulse lengths. The pattern of the subpeaks for

TABLE I. Table of results obtained from a plot of position of minima in the interference pattern against $(4q-1)^{2/3}$, where $q=1,2,3,\ldots$, pulses of angular frequency $\omega=0.182$ and electric field $E=0.053$ and varying pulse lengths.

Cycles in pulse	Gradient, G	$GN^{2/3}$	W_p(max)
64	$(5.06\pm0.13)\times10^{-3}$	0.081 ± 0.002	0.0325 ± 0.0005
128	$(3.25\pm0.07)\times10^{-3}$	0.081 ± 0.004	0.0325 ± 0.0007
240	$(2.06\pm0.11)\times10^{-3}$	0.080 ± 0.004	0.0322 ± 0.0005

TABLE II. Table of results obtained from a plot of position of minima in the interference pattern against $(4q-1)^{2/3}$, where $q=1,2,3,\ldots$, for pulses of angular frequency $\omega=0.182$, a pulse length of 64 cycles of the laser field, and for varying electric fields.

Electric field	Gradient, G	$GE_0^{-2/3}$
0.048	$(4.87\pm0.20)\times10^{-3}$	0.037±0.002
0.053	$(5.06\pm0.13)\times10^{-3}$	0.036±0.001
0.060	$(5.30\pm0.15)\times10^{-3}$	0.036±0.001
0.064	$(5.53\pm0.14)\times10^{-3}$	0.035±0.001
0.068	$(5.84\pm0.14)\times10^{-3}$	0.035±0.001

the higher ATI peaks (not shown here), is similar, as expected at this intensity. If the value for the maximum Stark shift is taken simply as $-(E_0^2/4\omega^2)$ as suggested by Eq. (3.3), with $t=T/2$, then it is found that the above theory predicts maxima and minima at points that are displaced by a small amount (of the order of $\omega/50$) with respect to the observed maxima and minima. This displacement is constant for each subpeak and is the same value for each of the main peaks in the energy spectrum. This small discrepancy between theory and observation arises because of the approximation involved in using $-(E_0^2/4\omega^2)$ as the maximum Stark shift. It has been pointed out by many authors[18] that this expression is only an approximation to the maximum Stark shift in the field and so it is no surprise that a small discrepancy arises between the theoretical prediction and the observed positions. However, this does not invalidate any of the predictions for the relative positions of the subpeaks for each main peak, because the separation of the subpeaks is dependent only on the small *time-dependent variation* of the Stark shift near the peak of the pulse and not on its absolute magnitude. Hence adjusting the absolute value of the maximum Stark shift is justified and does not affect the relative positions of the subpeaks. Table I gives the values of the maximum Stark shift of the ground state obtained from the plots and the results show that the value of this shift is independent of pulse length, as expected. Table I also shows the gradient G of a plot of the positions of the minima of the patterns against $(4q-1)^{2/3}$ for the three pulses of Fig. 1. As can be seen, the values of $GN^{2/3}$ yield consistent results that are very close to the predicted value of 0.079. If a log plot of the ATI peak is examined, it can be seen that, for values of q approximately greater than 6, the theory predicts a subpeak separation that is slightly more than that observed. This is to be expected as the approximation of Eq. (3.11) becomes less valid as the time from the center of the pulse increases.

The subpeak positions also show a dependence on the peak electric field of the pulse that is consistent with the theory developed above. The results of calculations for varying peak electric fields and identical angular frequencies and pulse lengths are summarized in Table II. The value for $GE_0^{-2/3}$ for the various electric fields is comparable with that of 0.0348 predicted by the theory. As we said earlier, the simple theory that we have developed is only valid for fields below the critical-field intensity where over-the-barrier ionization cannot occur. We have analyzed quantum-mechanical interference spectra for intensities up to this critical-field intensity and, close to this intensity, the agreement with the predictions is good for the higher-order peaks (one or more extra photons absorbed). However, for the first or second ATI peaks, there are some discrepancies. It has been pointed out that there are many different mechanisms in strong fields by which the continuum population can be modified.[19] Our model assumes that the continuum is populated directly from an isolated bound state. If other competing processes exist at high-field strengths that populate the lower part of the continuum, then there would be considerable deviations from the predicted pattern.

Figure 2 is an example of the large number of interference peaks that are obtained for smaller frequencies. The width for which peaks are visible is over half the main peak separation. There are no noticeable resonances occuring in this spectrum. This is the lowest angular frequency at this intensity for which there is a clear interference pattern. We will explain the existence of this lower limit in Sec. IV.

As stated, the theory developed above applies to regions of parameter space where there are no resonances in the spectrum to affect the interference pattern. When resonances exist, they modify the ATI spectrum as we will show in Sec. IV.

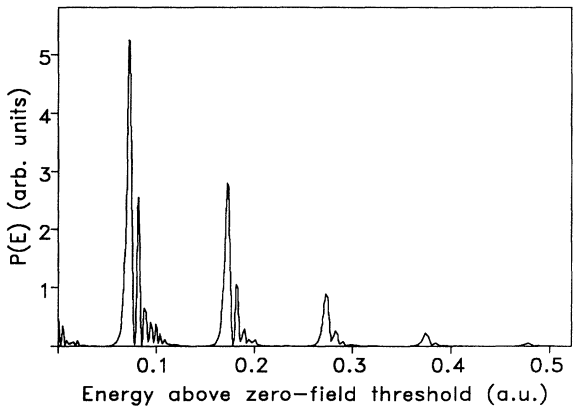

FIG. 2. Energy spectrum from a 64 cycle (97 fs) pulse of angular frequency $\omega=0.100$ (456 nm) and peak electric field, $E_0=0.053$ ($\approx10^{14}$ W/cm^2).

IV. THE INFLUENCE OF GROUND TO BOUND-STATE MULTIPHOTON RESONANCES

When a plot of the ionization yield as a function of angular frequency is examined, for a specific peak intensity and number of laser cycles per pulse, then in addition to the discontinuities arising from the change over from n to $(n+1)$ photon ionization, there are also peaks in the total ionization that correspond to an enhancement of the ionization rate due to the occurence of a bound-state resonance (Fig. 3).

Because of the time-varying electric field, the Stark shifts of the various bound levels in the atom are also time varying. This leads to transient multiphoton resonances occuring at various points in the pulse and the theory outlined in Sec. III becomes invalid near them because of the angular-frequency dependence of the coupling factor V_{gc}, which was previously taken as constant.

For the higher frequencies (≈ 5 photon resonance or less), the transient resonances are isolated, i.e., at most only one identifiable resonance occurs in a pulse at the intensities that have been used in this paper, and these resonances can be easily observed by their effect on the ATI spectrum. In Fig. 4, the effect of a multiphoton resonance in the ATI spectrum is illustrated. A 32-cycle, 10^{14} W/cm^2 pulse is examined and because of the short pulse length, any interference structure to the main peak is small. When the pulse is tuned to below the resonance [Fig. 4(a)], then a second small peak can be seen to the right of the ATI peak with a long tail on its right-hand side. This second peak is an interference peak, but the long tail is due to the resonance in the spectrum at this energy in the continuum. As the angular frequency of the laser is increased, the position of the resonance in the energy spectrum remains approximately constant, but its magnitude increases. The ATI peak position is, however, angular-frequency dependent and moves closer to the resonance peak [Fig. 4(b)]. Then as the detuning of the laser decreases still further, the main ATI and resonance peaks begin to merge [Fig. 4(c)]. As the angular frequency is increased still further into exact resonance, the ionization is significantly enhanced and only one peak is visible [Fig. 4(d)]. At this point, one of the higher bound states of the atom is exactly in multiphoton resonance with the ground state at the peak of the pulse. Examining the spectrum on a log plot, one can still see the interference structure to the right of the enhanced peak, but it is negligible in magnitude compared to the resonantly enhanced main ionization peak. With increased detuning above the bound level, the two peaks separate. The magnitude of the resonance peak drops rapidly and the interference pattern becomes comparable in size to the resonance peak [Fig. 4(e)]. With further detuning, the resonance peak size further decreases until it disappears altogether.

Obviously, the peak ionization rate occurs when the laser is tuned exactly to resonance and this allows for the determination of the bound state that is in resonance. In the model atom that has been used and for the intensities being dealt with here, the Stark shift of the bound levels with respect to the continuum is small for all the bound levels except the ground state. The unshifted energies are therefore reasonable approximations to the true energies in the electric field and using expression (3.9) for the ground-state shift, one can identify the resonant levels. Justification for using these unshifted excited levels of the atoms can be found in the close correlation of the observed resonance positions with those predicted by this zeroth-order approximation. If the excited levels are only very slightly shifted by the electric field, then the position of the resonant peak in the energy spectrum would be independent of the degree of detuning and only the magnitude of the peak would vary. This is found to be true to a good approximation and hence justifies the use of the unperturbed energies.

Table III shows four of the most dominant resonances detected by increases in the ionization yield and merged peaks in the ATI spectrum. The angular frequencies at which these resonances occur are compared with those predicted by using unshifted excited states of the atom relative to the continuum and describing the shift of the ground state of the atom by Eq. (3.9). It can be seen that the correlation of the predicted and observed positions is

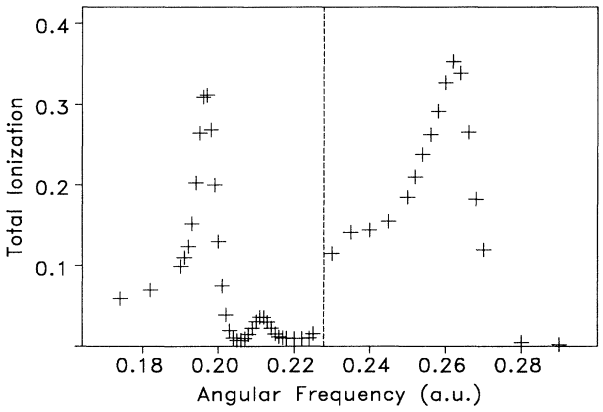

FIG. 3. Graph of total ionization yield as a function of angular frequency for a 32 cycle pulse, with electric field 0.053. Each cross represents a calculated yield and the dashed line marks the changeover from three- to four-photon ionization.

TABLE III. Table of positions of the observed maxima in the plot of total ionization as a function of angular frequency, which correspond to the occurence of multiphoton resonances between the Stark-shifted ground state and the excited states of the model atom. The observed values of the angular frequencies are compared with those predicted using unshifted excited states and a ground-state Stark shift given by Eq. (3.3).

Quantum number	n-photon resonance	Predicted ω	Observed ω
4	3	0.198	0.196±0.001
6	3	0.213	0.211±0.001
3	2	0.264	0.262±0.001
5	2	0.307	0.306±0.002

good and the assignment of specific levels to the resonances is justified. Of course, the validity of assigning quantum numbers to the bound-state resonances is limited by the intensity of the incident field. At the intensity that we have employed here, the ac Stark shift of the ground state with respect to the continuum is adequately described by the expression for the ponderomotive shift and the shifts of the higher bound states are small.

A further complication can exist because the width of a bound state in an external field is increased by the field. When this width is comparable to the spacing between adjacent levels we must consider these levels to be strong-

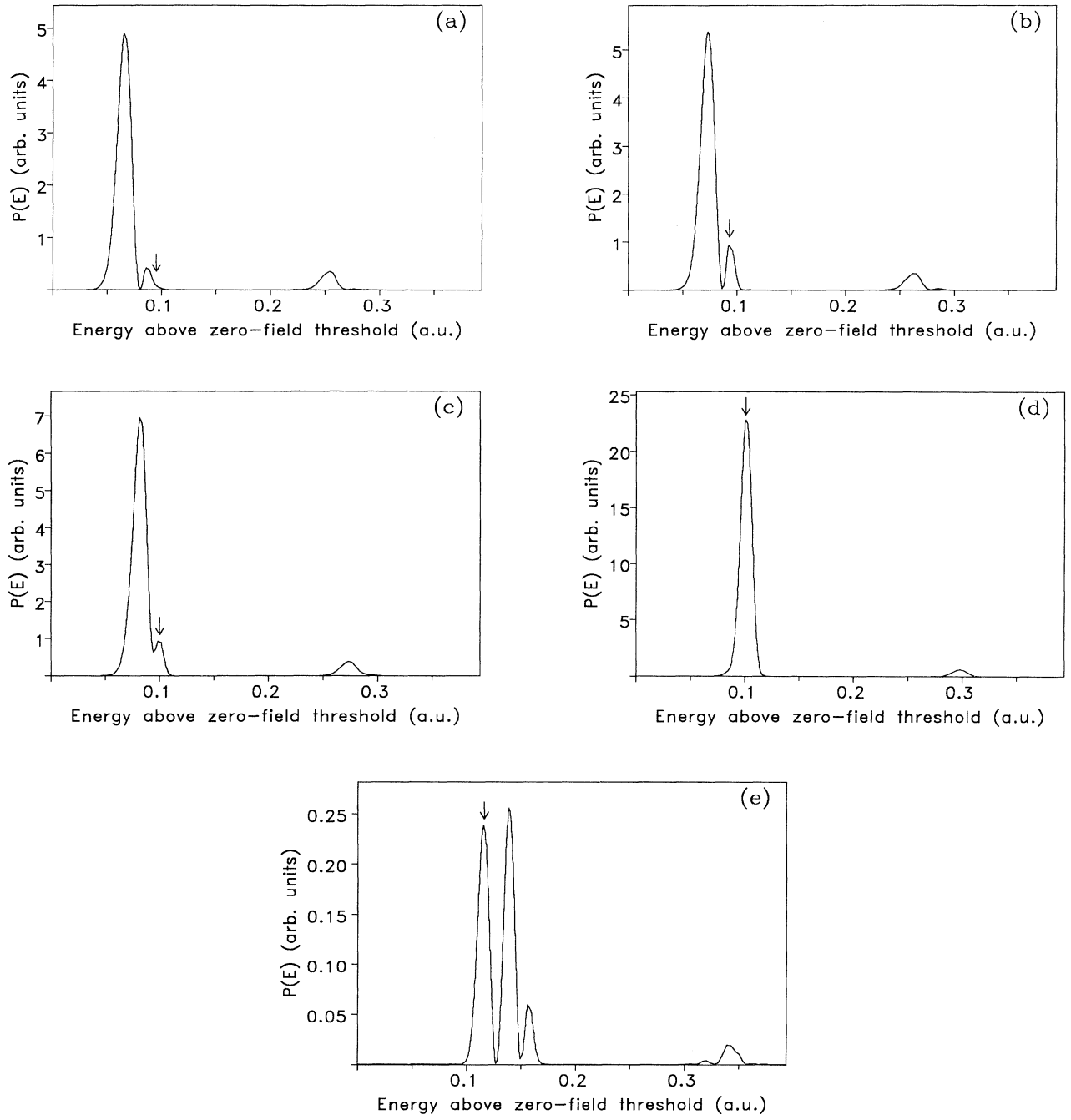

FIG. 4. Energy-spectrum graphs showing the effects of resonances in the ATI spectrum for pulses of peak electric field $E_0=0.053$ ($\approx 10^{14}$ W/cm^2) and 32 cycles. Angular frequencies are (a) 0.188 (242 nm), (b) 0.190 (240 nm), (c) 0.192 (237 nm), (d) 0.197 (231 nm), (e) 0.205 (222 nm). The arrows mark the positions of the resonance peak.

ly mixed. Such mixing occurs initially in the higher levels of the atom, where the level spacing is smallest, but as the incident electric-field strength increases, the region of the mixing moves lower.

When an atom ionizes nonresonantly at low field intensities, the electron passes through a series of virtual energy levels. At higher fields, when one of these energy levels lies within the region of mixing, then the level can be considered as real and the resultant ATI spectrum can be affected because the energy conserving points in the spectrum are now decided by the intermediate excited states.

This bound-state mixing also contributes to the breakdown at low frequencies of the theory presented earlier for the production of a quantum-mechanical interference pattern. At a given intensity the energy levels of an electron in a low-frequency field are obviously closer together than those in a high-frequency field. Therefore at low frequency, one of the energy levels will always lie within the mixed-level region of the atom. This, together with the fact that at smaller angular frequencies the larger ponderomotive shift will sweep more of the bound states into resonance, means that at lower frequencies, the photoelectron spectra are considerably more complicated.

At the electric-field strength considered here, the sharpness of the resonances in Fig. 3 indicates that high-level mixing plays little part in the ionization. It is also noticeable that the most dominant resonances that occur are those where parity conservation is observed. This is a rather surprising result because one might expect parity to be no longer a good quantum number in fields of this intensity. We would point, out, moreover, that our results compare well, in the relevant region, with those of Sundaram and Armstrong who use an implicitly parity-violating potential.[19] Parity conservation is therefore not an overriding consideration in the problem: it does, however, give a good indication of those routes that will dominate the ionization.

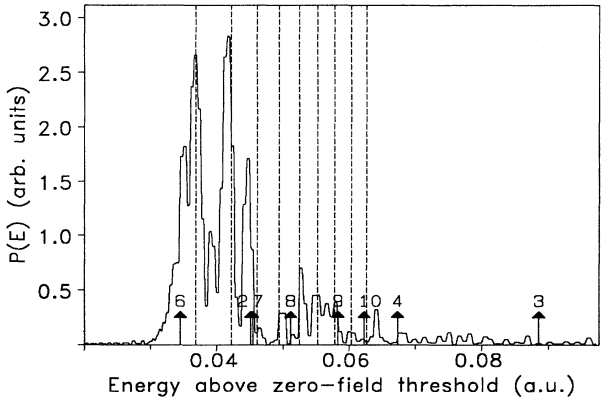

FIG. 5. Plot of the first ATI peak in the energy spectrum from a 150 cycle (0.285 ps) pulse of angular frequency 0.08 (570 nm) and peak field intensity $E_0=0.053$ ($\approx 10^{14}$ W/cm^2). The dotted lines mark the predicted positions of the rainbow peaks and the arrows mark where peaks from bound-state resonances would be expected.

As the angular frequency decreases, the shift in energy of the ground state for a particular electric-field strength becomes larger and so more of the excited levels can be swept into resonance during a pulse. This makes the identification of the various peaks in the field more difficult. For short pulse lengths, the rainbow structure of the spectrum is still very noticeable but as the pulse length increases, the resonances increase in magnitude and the spectrum appears to be a mixture of various resonances and structure that corresponds to that produced by quantum-mechanical interference (Fig. 5).

As can be seen from Fig. 5, not all the peaks in the spectrum can be attributed to resonances and the occurence of quantum-mechanical interference must be considered when interpreting the spectrum. In an actual experiment, the spatial extent of the beam must be taken account of and this may lead to some degree of averaging of the spectra produced at the varying intensities across the width of the laser beam. Such averaging would possibly lead to a "smearing" of the interference pattern. However, it is not the purpose of this paper to investigate the effect of the spatial dependence of the electric field, but instead to point out that there are effects arising because of the time-varying electric-field envelope that must be included in the full treatment of the phenomenon.

V. CONCLUSION

It has been shown that both multiphoton resonance ionization and quantum-mechanical interference play a part in determining the detailed shape of peaks in ATI spectra. Depending on the exact frequency and structural details of the atom, either of these two effects may be dominant, or for longer wavelengths, both may play a part. The analysis of actual spectra obtained by experiment must therefore contain elements of both to represent all the effects of a time-dependent laser pulse.

For spectra from the higher-frequency regime where resonances either do not occur or only occur in isolation, the analysis becomes easier and each aspect of the spectrum is readily identifiable. For the lower frequencies, where more resonances can occur in one pulse, the pattern of the energy spectrum becomes more complicated and includes elements both of the interference pattern and resonance peaks.

The spectra presented in this paper are all produced by a single smooth electric-field envelope. In an actual experiment obviously the spatial variation of the electric field across the beam, and temporal fluctuations of the pulse, cause the actual spectra produced to be some average of a series of spectra. But it can be imagined that because of the width and magnitude of the interference pattern, then some remnant of the smeared pattern may still be noticeable. The effect of this spatial averaging would not be as noticeable on the resonance peaks, because of the weaker dependence on the electric field of the position of these peaks.

Further work is at present being carried out on the effect of spatial averaging on the pattern. Recent experi-

ments producing ATI spectra from atomic hydrogen[20] have yielded spectra of a similar type to that of Fig. 5, and work has been carried out to identify the peaks in this experimentally obtained spectrum using time-independent Floquet theory.[5] It will be interesting to see whether using time-dependent calculations will introduce further effects into the spectrum.

ACKNOWLEDGMENTS

We thank Professor P. L. Knight and Dr. M. Dörr for helpful discussions. One of us (V.C.R.) acknowledges the support of STC Technology Limited. This work is part of a research program supported by the Science and Engineering Research Council (SERC).

[1]P. Agostini, A. Antonetti, P. Breger, M. Crance, A. Migus, H. Muller, and G. Petite, J. Phys. B **22**, 1971 (1989).

[2]R. R. Freeman, P. H. Bucksbaum, H. Milchberg, S. Darack, D. Schumacher, and M. E. Geusic, Phys. Rev. Lett. **59**, 1092 (1987).

[3]H. G. Muller, H. B. van Linden van den Heuvell, P. Agostini, G. Petite, A. Antonetti, M. Franco, and A. Migus, Phys. Rev. Lett. **60**, 565 (1988).

[4]For example, Shih-I Chu and J. Cooper, Phys. Rev. A **32**, 2769 (1985); R. Shakeshaft and R. M. Potvliege, *ibid.* **36**, 5478 (1987); H. Gratl, G. Alber, and P. Zoller, J. Phys. B **22**, L547 (1989).

[5]R. M. Potvliege and R. Shakeshaft, Phys. Rev. A **41**, 1609 (1990); R. M. Potvliege and R. Shakeshaft, Phys. Rev. A **40**, 3061 (1989); M. Dörr, Ph.D. thesis, University of Southern California, 1990.

[6]V. C. Reed and K. Burnett, Phys. Rev. A **42**, 3152 (1990).

[7]J. Javanainen, J. H. Eberly, and Qichang Su, Phys. Rev. A **38**, 3430 (1988).

[8]For example, J. N. Bardsley, A. Szöke, and M. J. Comella, J. Phys. B **21**, 3899 (1988); K. C. Kulander, Phys. Rev. A **38**, 778 (1988); P. Lambropoulos, A. Lyras, and X. Tang, in *Fundamentals of Laser Interactions II,* edited by F. Ehlotzky, Lecture Notes in Physics Vol. 339 (Springer-Verlag, New York, 1989), p. 3.

[9]K. Burnett, P. L. Knight, B. Piraux, and V. C. Reed, Phys. Rev. Lett. **66**, 301 (1991).

[10]M. Pont, N. R. Walet, and M. Gavrila, Phys. Rev. Lett. **61**, 939 (1988); M. Pont and M. Gavrila, Phys. Rev. Lett. **65**, 2362 (1990).

[11]Q. Su, J. H. Eberly, and J. Javanainen, Phys. Rev. Lett. **64**, 862 (1990).

[12]R. Bhatt, B. Piraux, and K. Burnett, Phys. Rev. A **37**, 98 (1988).

[13]H. A. Kramers, *Collected Scientific Papers* (North-Holland, Amsterdam, 1956), p. 272.

[14]W. C. Henneberger, Phys. Rev. Lett. **21**, 838 (1968).

[15]W. H. Press, B. P. Flannery, S. A. Teukolsky, and W. T. Vetterling, *Numerical Recipes* (Cambridge University Press, Cambridge, England, 1987).

[16]M. V. Berry and K. E. Mount. Rep. Prog. Phys. **35**, 315 (1972); P. T. Greenland, J. Phys. B **18**, 410 (1986); M. A. Lauder, P. L. Knight, and P. T. Greenland, Opt. Acta **33**, 1231 (1986); M. A. Lauder and P. T. Greenland, J. Phys. B **17**, 3083 (1984); P. A. Rodgers and S. Swain, J. Mod. Opt. **36**, 941 (1989).

[17]S. Augst, D. Strickland, D. D. Meyerhofer, S. L. Chin, and J. H. Eberly, Phys. Rev. Lett. **63**, 2212 (1989).

[18]For example, P. W. Milonni, and J. R. Ackerhalt, Phys. Rev. A **39**, 1139 (1989); L. W. Pan, L. Armstrong, Jr., and J. H. Eberly, J. Opt. Soc. Am. B **3**, 1319 (1986).

[19]B. Sundaram and L. Armstrong, Jr., Phys. Rev. A **38**, 152 (1988); B. Sundaram and L. Armstrong, Jr., J. Opt. Soc. Am. B **7**, 414 (1990); see also S. M. Susskind and R. V. Jensen, Phys. Rev. A **38**, 711 (1988).

[20]H. Rottke, B. Wolff, M. Brickwedde, D. Feldman, and K. H. Welge, Phys. Rev. Lett. **64**, 404 (1990).